Z. Phys. Chem. **217** (2003) 1613–1626

Influence of Cation Exchange on the ^{27}Al-NMR Spectra of Zeolites

By W. Masierak[1], T. Emmler[2], G. Buntkowsky[2,*], and A. Gutsze[1,*]

[1] Medical Academy of Bydgoszcz, Department of Biophysics, ul. Jagiellonska 13, Bydgoszcz, Poland
[2] Freie Universität Berlin, Institut für Chemie, Takustraße 3, 14195 Berlin, Germany

Dedicated to Prof. Dr. Hans-Heinrich Limbach on the occasion of his 60th birthday

(Received May 28, 2003; accepted in revised form September 4, 2003)

NaA-Zeolite / ^{27}Al-MAS-NMR / Quadrupol Coupling Constants

The influence of cation exchange on the ^{27}Al-NMR spectra of NaA-zeolites has been studied by ^{27}Al-MAS- and MQ-MAS-Solid State-NMR. From the ^{27}Al-spectra a characterization of the different Al sites in the A zeolites according to their chemical environment and the structural changes on the aluminosilicate network caused by the cation exchange are obtained. It is found that the exchange with cations with smaller ion-radius cause stronger distortions of the ^{27}Al-NMR-spectra than exchange with larger cations like Ba^{2+}. Employing MQ-MAS spectroscopy these distortions are revealed as second order quadrupolar effects for the smaller cations and as a combination of chemical shift and second order quadrupolar interaction for the Ba cation. These changes of the quadrupolar coupling are interpreted numerically via calculations of the lowering of the symmetry of the EFG tensor. Finally it is found that the exchange with divalent cations leads to distortions of the zeolitic framework and the formation of an extra-framework aluminum. To the best of our knowledge this is for the first time that evidence for the production of extra frame work aluminum by pure cation exchange without any thermal treatment has been found in type A zeolites.

1. Introduction

Zeolites are porous, crystalline materials which belong to the class of aluminosilicates. The structure of zeolites consists of SiO_4^{4-} and AlO_4^{5-} tetrahedra, linked together by sharing oxygen atoms [1, 2]. They are employed as synthetic molecular sieves that are of special interest because of their selective adsorptive properties. These selective adsorptive properties are due to a porous

* Corresponding authors. E-mail: bunt@chemie.fu-berlin.de

crystal structure incorporating interconnecting channels and cavities of definite and uniform size. Molecules having appropriate size and shape can enter these channels and be adsorbed in the internal cavities [3, 4]. After the seminal discovery of the MQMAS technique by Frydman in 1995, the study of zeolites and related material by solid state NMR has grown fresh impetus [5–10].

Zeolites type A, which are studied in this work, are characterized by a Si/Al ratio equal to 1. The negative electrostatic charge of the aluminosilicate network, which is proportional to the number of $(AlO_2)^-$ groups, is neutralized by Na^+ cations occupying the zeolite cavities. These sodium cations are bounded only by electrostatic forces. They can be easily exchanged with other mono- or bivalent cations. The charge-compensating cation exchange causes changes of the electrostatic field inside the large cavities. This field plays an important role in the absorption of molecules inside the zeolites [11]. Thus the cation exchange controls the physicochemical properties of the zeolites [12]. Another aspect of the ion exchange is that the molecular sieving action of zeolite A is strongly influenced by the size of cations located on the eight-ring windows [13]. For example by cation exchange pore diameters can be adjusted in such a way that molecules of different size and shape are separated. However the cation size is not the only parameter which plays a role. Exchanging the monovalent Na^+-cations with multivalent cations causes vacancies in the charge distribution and thus reduces its symmetry. This results in a local increase of the electrostatic field inhomogeneity, rendering the adsorbent less energetically homogeneous [14]. If only monovalent cations are present the maximum homogeneity is achieved. Multivalent cation exchange is usually accompanied by the development of hydroxyl groups. The arrangement and the nature of these hydroxyl groups are another important factor, which influences the properties of zeolites A as molecular sieves and adsorbents [15].

Studies of sorption and desorption of *n*-paraffin on zeolites type A show the existence of transport resistances on the surface of crystallites of zeolites [16]. Those so called 'surface barriers' become more significant after a hydrothermal pretreatment of the NaCa-A zeolite. NMR studies on the aluminosilicate framework of the thermally pretreated Calcium exchanged zeolite led to the conclusion that cation exchange together with thermal treatment leads to the formation of aluminosilicate skeleton defects. These defects are interpreted as the presence of extra-framework aluminum [17]. This effect is not observed with monovalent cation exchanged zeolites A [18].

It is well known that the nuclear quadrupolar moment is a very sensitive sensor of the local electric field close to a quadrupolar nucleus. Thus, by NMR experiments performed on the ^{27}Al nuclei, which have a large nuclear quadrupolar moment, one can detect modifications of the electric field inside zeolite A cavities due to cation exchange. In principle also the chemical shift of another quadrupolar nucleus in the zeolite framework – ^{17}O is also dependent on the charge-compensating cation exchange [19],

however these experiments would necessitate an isotope enrichment with ^{17}O nuclei.

The main goal of this work is the investigation of the influence of ionic radii of the charge-compensating cation on the electric field distribution in the zeolites A, employing the quadrupolar ^{27}Al nuclei as sensitive monitors for their surrounding electric field. Furthermore we have investigated whether the dealumination and defect formation, which causes the presence of extra-framework aluminum, can be initiated solely by cation exchange without any thermal treatment.

2. Experimental section

2.1 Synthesis and sample preparation

The parent NaA zeolite was synthesized following the procedure given in the literature [20]. Special care was taken to obtain a Fe content below 50 ppm. The calcium exchanged zeolite was obtained by Ca^{2+} ion exchange from $CaCl_2$ solution, using 20 cm^3 of nominally 0.1 mol salt solution per 1 g of zeolite at room temperature and constant agitation. The exchange procedure was repeated three times. A similar procedure was used to obtain zeolites exchanged with other cations like: Zn^{2+}, Ba^{2+}, Cd^{2+}, K^{1+}, Rb^{1+}, Li^{1+}. The degree of cation exchange was controlled by chemical analysis. For all samples an exchange rate larger than 99% was achieved. All samples were fully hydrated.

2.2 NMR spectroscopy

The cation exchanged zeolite samples were filled into standard 4 mm Chemagnetics pencil rotors. The ^{27}Al-MAS NMR spectra were recorded on a 600 MHz Varian Infinity Plus spectrometer, operating at an ^{27}Al resonance frequency of 156.33 MHz. All spectra were recorded employing a 4 mm Chemagnetics T3 MAS Probe. The MAS spinning frequency was controlled by a Chemagnetics MAS speed controller. The NMR spectra were recorded with NMR pulses between 1.2 and 1.7 μsec pulse width. These values are short enough to ensure a uniform excitation of the spectrum. The recycle delay between the scans in the accumulation was 0.1 sec. All ^{27}Al-solid state NMR spectra are referenced to an 0.1 M aqueous solution of $AlCl_3$, which was measured as external standard.

All MQ-MAS spectra were measured at room temperature at spinning speeds of 16.000 ± 0.005 kHz. Spectra were recorded employing the 3QZ_H-pulse sequence supplied with the spectrometer. Width of the pulses were 4 usec for the first and 1.4 usec for the second mq-pulse. The evaluation of the MQ-MAS spectra was performed employing the Hyper Shear I^+ macro supplied with the spectrometer.

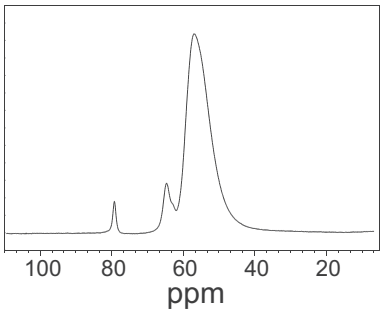

Fig. 1. Experimental ^{27}Al MAS-NMR spectrum of zeolite CaA.

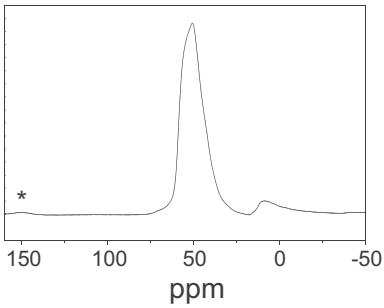

Fig. 2. ^{27}Al MAS-NMR spectrum of the zeolite ZnA.

3. Experimental results

3.1 1-D spectra

The set of fully hydrated zeolites type A with different charge-compensating cations was investigated by ^{27}Al MAS NMR. To control the reproducibility all spectra were measured at least two times.

Fig. 1 shows the MAS spectrum of the zeolite CaA. Three signals are observed. There is one sharp line at 79.24 ppm and two broad overlapping lines at 57 ppm and 64 ppm respectively. The MAS NMR spectrum of Zn^{2+} exchanged zeolite A is shown in Fig. 2. The spectrum consists of two resonance lines at 50.5 ppm and 10.2 ppm. Measurements performed at different rotating speeds (not shown) prove, that the line at 10 ppm is not formed by spinning sidebands. We attribute this line to a broad, slightly asymmetric (*i.e.* non-Lorentzian or Gaussian) distribution of aluminum sites with different chemical shifts or quadrupolar coupling constants.

For the zeolite CdA (with six Cd^{2+} cations) several partially overlapping lines are observed. As it is shown on Fig. 3 this line shape consists of a broad asymmetric line at 54 ppm with a shoulder at 63 ppm, a relatively sharp line at

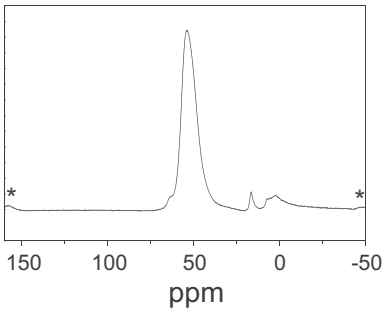

Fig. 3. Experimental ^{27}Al MAS-NMR spectrum of the zeolite CdA.

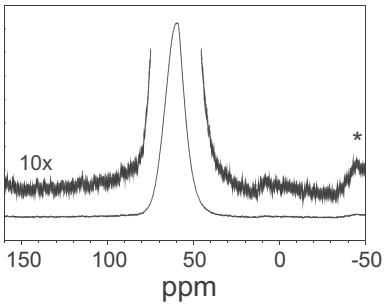

Fig. 4. ^{27}Al MAS-NMR spectra of the zeolite BaA. Note the small line at *ca.* 10 ppm visible in the magnification.

16.9 ppm and two overlapping lines at 7.2 ppm and 2.8 ppm. Measurements at different rotation speed (not shown) proved that all lines are caused by different types of alumina and exclude any assignment problems by spinning side bands.

Fig. 4 finally shows the NMR line of the zeolite A exchanged with Ba^{2+}, the largest cation in our study. In this case the spectrum consists mainly of a single broad line at 59.3 ppm. In addition the magnification of the spectrum shows again small line at *ca.* 10 ppm.

3.2 MQ-MAS spectra

From the 1D-spectra it is not possible to obtain reliable information about the chemical shifts of the Al-nuclei, owing to second order quadrupolar interaction. Therefore MQ-MAS spectra were recorded. Spectral data obtained from the MQ-MAS spectra are collected in Table 1. As examples of these MQ-MAS spectra we present the results on Calcium, Cadmium, and Barium.

Fig. 5 shows the MQ-MAS spectrum of the Calcium exchanged zeolite. From the projection on the isotropic chemical shift axis it is evident that

Table 1. Collection of quadrupolar coupling constants and isotropic chemical shifts obtained from the evaluation of the MQ-MAS spectra. [+)] For the CaA Zeolite the C_Q-value of the main line is given. [++)] For the BaA Zeolite all quadrupolar constants coincide in the margin of error.

^{27}Al Isotropic chemical shifts and quadrupolar constants of monovalent cations				
	Zeolite	Ionic radius [Å]	Isotropic chemical shift [ppm]	C_Q [MHz]
1	LiA	0.68	63.2	2.81 ± 0.17
2	NaA	0.97	61.2	2.25 ± 0.14
3	KA	1.33	59.5	2.21 ± 0.14
4	RbA	1.47	59.3	2.14 ± 0.13
5	CsA	1.67	58.9	1.67 ± 0.10

^{27}Al Isotropic chemical shifts and quadrupolar constants of divalent cations									
	Zeolite	Ionic radius [Å]	Isotropic chemical shift [ppm]						C_Q [MHz]
1	CaA	0.99	62.0		65.3		79.4		4.48[+)]
2	ZnA	0.74			59.5				6.18
3	CdA	0.97			59.9				4.67
4	BaA	1.34	62.3	64.3	67.2	70.1	73.5	76.0	4.15[++)]

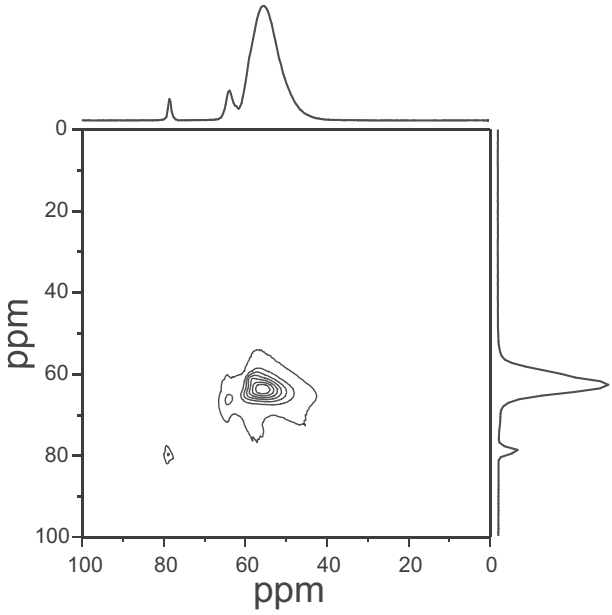

Fig. 5. Sheared ^{27}Al 3-MQMAS spectrum of the zeolite CaA.

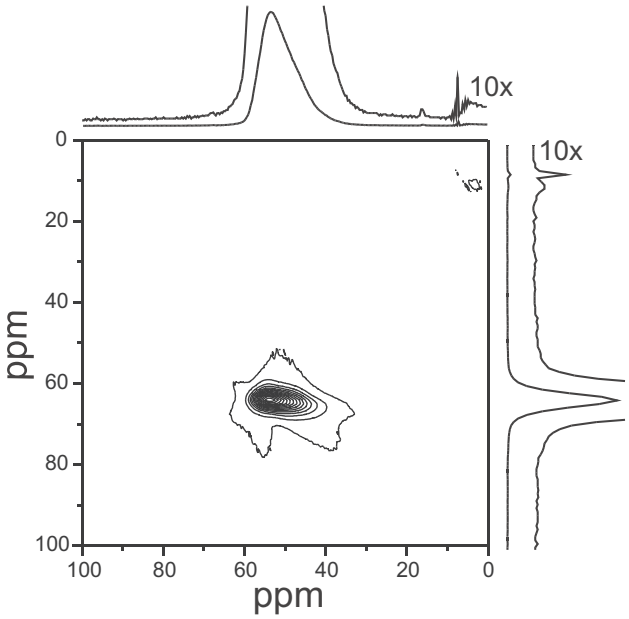

Fig. 6. Sheared ^{27}Al 3-MQMAS spectrum of the zeolite CdA.

the broad asymmetric line observed at 62 ppm is caused by a distribution of quadrupolar coupling constants. The isotropic chemical shift for this line is 62 ppm. There are additional smaller lines at 65.3 ppm and 79.4 ppm.

Fig. 6 shows the MQ-MAS spectrum of the Cadmium exchanged zeolite. From the projection on the isotropic chemical shift axis it is evident that the broad asymmetric line observed at 54 ppm is caused by a distribution of quadrupolar coupling constants. The isotropic chemical shift for this line is 59.9 ppm. There are additional small lines at 13 ppm, visible in the enlargement of the isotropic dimension.

Fig. 7 shows the MQ-MAS spectrum of the Barium exchanged zeolite. Here a structure of the broad component is visible in both dimensions, suggesting a distribution of both quadrupolar couplings and chemical shifts. From the MQ-MAS spectrum six different line positions at 62.3, 64.3, 67.2, 70.1, 73.5 and 76.0 ppm are elucidated inside the broad component. In addition there is a smaller line at *ca.* 10 ppm.

4. Discussion

Our main goal is the characterization of the different Al sites in the A zeolites according to their chemical environment and the structural changes on the

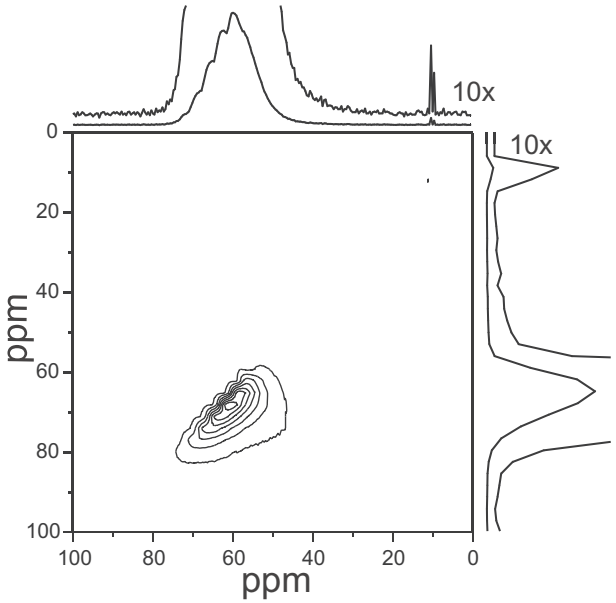

Fig. 7. Sheared ^{27}Al 3-MQMAS spectrum of the zeolite BaA.

aluminosilicate network caused by the cation exchange. In a first step we therefore have to attribute the various ^{27}Al-MAS-NMR lines to different chemical species of aluminum.

4.1 CaA-zeolite

The zeolite type A consists of AlO_4 and SiO_4 tetrahedra [21] thus for NaA zeolite only one narrow MAS NMR line is observed. According to its chemical shift of 62 ppm this line is assigned to the tetrahedrally coordinated aluminum nuclei [22]. The additional line at 65.3 ppm, which appears after substitution of Na^{1+} with Ca^{2+} has a chemical shift value which is inside of the typical range of framework aluminum (65–51 ppm). Thus it may be assigned to framework aluminum near hydrated Ca^{2+}. The third line at 79.4 ppm has a chemical shift close to the value measured for a $Al(OH)_4^-$ solution which exhibits a chemical shift of 80 ppm [23]. Therefore the third line in a CaA zeolite can be attributed to extra-lattice $Al(OH)_4^-$ anion, *i.e.* ions which are not part of the framework [18].

4.2 ZnA and CdA zeolites

The spectra of ZnA and CdA zeolites show two kinds of lines. First the line within the range of 50–64 ppm and second between 2.8 and 16.9 ppm. The

first region may be assigned to tetrahedral aluminum in the zeolite framework. From the MQ-MAS spectra it is evident that the chemical shift has a constant value of 59.5 ppm (Zn) and 59.9 ppm (Cd). Thus the apparent width and asymmetry of these lines is the result of a distribution of quadrupolar coupling constants. X-ray studies of CaA zeolites [24, 25] show a severe distortion of the 6-ring, due to Ca atom coordination to the ring. The same process may appear in ZnA and CdA zeolites and small distortions with a strain induced on the lattice may lead to these variations in the electric field gradient, which are necessary to account for the distribution of C_Q. The second region (2.8–16.9 ppm) may be assigned to the extra-framework aluminum which is under the influence of the divalent cations. This influence may be the reason for the shift from 0 ppm which is the normal chemical shift value of free octahedrally coordinated aluminum [22, 26, 27] to the values of 2.8–16.9 ppm observed in our sample. In addition to this strong line there is some intensity at *ca.* 10 ppm, which is an indication of extra frame work aluminum.

4.3 BaA-zeolite

Compared to the previous two examples the Barium exchanged zeolite exhibits an interesting difference. Here the cation exchange causes a splitting of the broad line into several sub-lines with different chemical shifts and not only a distribution of quadrupolar coupling constants, as found for the other zeolites.

4.4 Numeric simulation of EFG

The next question which arises is, what is the cause of the observed changes in the distribution and strength of the quadrupolar coupling constants, respectively the underlying electric field gradient tensor. The electrical field gradient on the different alumina sites is caused by the electric field of the neighboring silica and oxygen atoms plus the field of the charge compensating ions. The cation exchange can have a two-fold effect on the Al-spectra:

- The different cations have different sizes and charges, which changes the symmetry of the charge distribution and distances of the cations from the Al and thus directly the electric field gradient (direct effect)
- The cation exchange causes distortions in the arrangement of the oxygen tetrahedron neighboring the Al-ion, which causes an indirect change of the electric field gradient (indirect effect).

Both these effects will depend strongly on the symmetry of the distribution of these ions. In principle the $1/r^3$-dependence of the electric field gradient on the distance is in favor of the distortion of the oxygen tetrahedron, *i.e.* the indirect effect, but it is not clear, whether this is effect is stronger than the direct effect, due to the changes in the charge distribution.

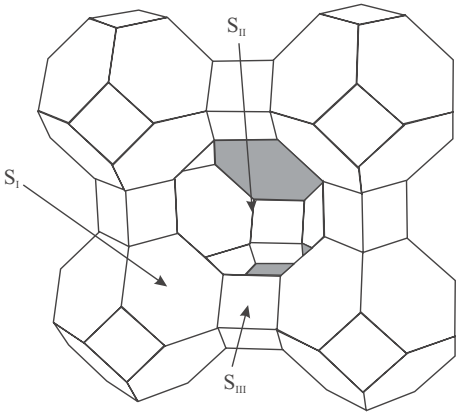

Fig. 8. Schematic representation of the possible cation locations in the zeolite type A.

To estimate the size of the different contributions for the different cations, we have numerically calculated the electric field gradient which is produced by exchangeable cations at the aluminum atom position employing a point charge model on the one hand and the effect of the distortion of the symmetry of the oxygen tetrahedron on the other hand. In this model the ions with charge q_k are placed on the crystallographic sites r_k inside the zeolite and their electric potential is calculated as:

$$V = \frac{1}{4\pi\varepsilon_0} \sum_k \frac{q_k}{\left|\vec{r}_k - \vec{r}_{\mathrm{Al}}\right|} . \tag{1}$$

Calculation of direct effect

In zeolites type A there are three possible locations of charge-compensating cations [11] called S_I, S_{II} and S_{III}. As shown in Fig. 8 the S_I sites are located close to the center of the six-membered oxygen rings of the aluminosilicate framework. The S_{II} sites are near the eight-membered oxygen rings (the plane of the pores leading to the cavities) and the S_{III} positions are in the large cavity opposite a 4-ring.

As the first system the unmodified NaA zeolite itself has been studied, which is the most symmetrical case. In the zeolite NaA there are 12 Na^+ cations per unit cell. There are fewer cations than atomic sites, however all 8 S_I positions are occupied, 3 S_{II} sites and one S_{III} site is occupied. All these positions have equal statistical probability and are distributed symmetrically in the zeolite cavity. For the numerical calculation of the electric field gradient the X-ray data of Howell [28] were employed. The crystal was modeled as twenty seven unit cells (three in each direction) and the field at the position of the central unit cell was calculated. According to Howell the S_I and

S_{II} positions are split into three equivalent, randomly occupied cation positions. Therefore the assumption has been used that all cation positions in our model compound are occupied by the same charge. Thus all cations at S_I positions are assigned a charge equal to $+0.3333$ e, the S_{II} cations are assigned a charge equal to $+0.125$ e and the S_{III} cations are assigned a charge equal to $+0.125$ e. The electric field gradient was calculated according to the following formula:

$$Q = \frac{\partial E_k}{\partial \chi_l} = \frac{\partial^2 V}{\partial \chi_k \partial \chi_l} \qquad k, l = x, y, z\,. \tag{2}$$

Under these assumptions we calculated first the gradient for the pure (*i.e.* unexchanged) zeolite. Since these calculations do not give the complete EFG, but only the additional part caused by the cations, they are not directly comparable to the experimental C_Q-value of the NaA Zeolite. The performed calculations predict a value of the electric field gradient q_{zz} equal to $0.4042\,\mathrm{V/Å^2}$ and an asymmetry parameter of $\eta = 0.56$ Next we have taken the same model but all Na^{1+} cations were replaced by Ca^{2+} cations. For one unit cell only 6 Ca^{2+} cations are needed to neutralize the negative charge of the aluminosilicate network, and divalent cations such as Ca^{2+}, Mg^{2+} and Ba^{2+} show site S_I selectivity [12, 13]. As a result the charge distribution is less symmetric as in the previous case. There are 8 S_I sites, each split into three possible cation positions. Under the assumption that the charge is uniformly distributed over all the possible cation positions, we decided to place a charge equal to $+0.5$ e in each possible S_I position. Such a charge distribution leads to a q_{zz} value equal to $1.2\,\mathrm{V/Å^2}$ and an asymmetry parameter $\eta = 0.61$. These results clearly demonstrate that the exchange of charge-compensating cations leads to changes in the electric field gradient at the Al site. Bivalent cations cause increasing electric field gradient and lower its symmetry.

The calculations of the contribution to the electric field gradient caused by charge-compensating cations show that bivalent cations produce less symmetrical and more than two times stronger electric field gradients than monovalent cations located at the same positions. Such a change in the electric field should be visible as a line broadening and in addition a shift of the line positions towards lower values of the chemical shift. Therefore it is interesting to compare the ^{27}Al-lines with respect to this expected line broadening and line shift: in the case of quadrupolar nuclei like ^{27}Al the center of gravity of the NMR line is shifted by quadrupolar interactions [22, 29, 30].

Calculation of the indirect effect

As mentioned above the cation exchange can also cause a distortion of the positions of the neighboring oxygen atoms, which reduces the tetrahedral symmetry of the oxygen cage and causes a second contribution to the EFG tensor. To estimate the size of this contribution the following assumptions were made:

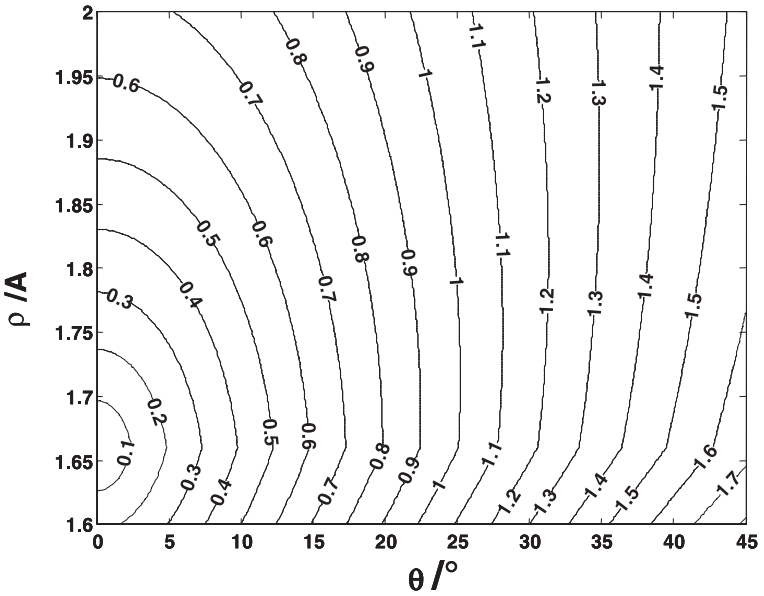

Fig. 9. Calculated EFG gradients in $V/Å^2$ as a function of the Al–O distance ρ and the deviation $\Delta\theta$ from the ideal tehtrahedral angle.

- In an idealized zeolite framework the oxygen atoms are located on the corners of an ideal tetrahedron. The Al-atom is located in the center of this tetrahedron with an Al–O distance of 1.66 Å [28]. In the real, hydrated zeolite NaA, the mean deviation of O–Al–O bond angles from the ideal value ($\theta = 109.47°$) is equal to 2.4° [31].
- The net charge is distributed equally over all oxygen atoms [11].
- The cation exchange changes the position of only one of the four oxygen atoms. Under this assumption the symmetry of the EFG is reduced to axial and can be parametrized by the distance of the distorted oxygen from the central aluminum (ρ) and by the deviation angle ($\Delta\theta$) of the Al–O vector from the symmetry axis of the EFG tensor, which is identical to the ideal tetrahedral axis.
- The distance between aluminum and oxygen changes only toward larger distances.
- The deviation $\Delta\theta$ from the ideal tetrahedral angle is below 10°. This value follows from the correlation between ^{27}Al chemical shifts and mean Al–O–Si angles reported by Lippmaa [32] $\delta_{CS} = -0,5\theta + 132$ ppm.

The resulting gradient is shown in Fig. 9. Assuming that the change in the Al–O distance is less than 0.25 Å the contributions of the oxygen atoms to the EFG can be estimated to be in the range of (0–0.6) $V/Å^2$.

Comparing the sizes of the additional field gradients produced by the two mechanisms, it is evident that both mechanisms are on the same order of magnitude, *i.e.* non-negligible. For monovalent cations the effects are of similar sizes. For bivalent cations, the EFG produced by the direct cation exchange is roughly twice as strong as the EFG produced by the oxygen atoms. Thus we can conclude that for the bivalent cations the lowering of the symmetry of the cations is more important than the distortion of the oxygen cage.

5. Conclusion

From the presented results the conclusion may be drawn that the cation influence on the aluminosilicate network depends on the cation's ionic radius value. This is particularly visible by comparison of the spectra of ZnA and CdA zeolites with BaA. Zeolites with smaller cations exhibit more distorted spectra than zeolites with a large cation like Ba. Employing MQ-MAS spectroscopy the distortions in the spectra of the small cations are revealed as changes in the quadrupolar coupling constant, which are translated via second order quadrupolar effects in the spectra. For the larger Ba-cation, the changes are a result of both second order quadrupolar coupling and chemical shift changes. The exchange with divalent cations leads to distortions of the zeolitic framework and the formation of an extra-framework aluminum. To the best of our knowledge this is for the first time that evidence for the production of extra frame work aluminum by pure cation exchange without any thermal treatment has been found.

Acknowledgement

The authors want to express their gratitude to the referee for his helpful comments, which helped them very strongly in finding a correct interpretation of their experimental results. W.M. wants to express his thanks to the European Union for a one year fellowship in the Marie-Curie program under the contract N° HPMT-CT-2000-00127. Financial support by the Polish Committee for Scientific Research N° 5P03B05920 and the Deutsche Forschungsgemeinschaft, SFB-448, is gratefully acknowledged.

References

1. D. W. Breck, *Zeolite Molecular Sieves, Structure Chemistry and Use*, John Wiley, New York (1974).
2. R. M. Barrer, *Hydrothermal Chemistry of Zeolites*, Academic Press, London (1982).
3. L. Broussard and D. P. Shoemaker, J. Am. Chem. Soc. **78** (1960) 1041.
4. P. Concepción-Heydorn, C. Jia, D. Herein, N. Pfänder, H. G. Karge, and F. C. Jentoft, J. Mol. Catal. A: Chemical **162** (2000) 227.

5. J.-P. Amoureux and M. Pruski, *Encyclopedia of Nuclear Magnetic Resonance*, Vol. 9, pp. 226, John Wiley & Sons, Ltd, Chichester (2002).
6. D. Freude,T. Loeser, D. Michel, U. Pingel, and D. Prochnow, Solid State NMR **20** (2001) 46.
7. T. Loeser, D. Freude, G. T. P. Mabande, and W. Schwieger, Chem. Phys. Lett. **370** (2003) 32.
8. L. J. Smith, H. Eckert, and A. K. Cheetham, J. Am. Chem. Soc. **122** (2000) 1700.
9. L. J. Smith, H. Eckert, and A. K. Cheetham, Chem. Mater. **13** (2001) 385.
10. L. van Wüllen and G. Schwering, Solid State NMR **21** (2002) 134.
11. J. A. Michelena, E. F. Vansant, and P. de Bievre, Recl. Trav. Chim. Pays-Bas **97**(6) (1978) 162.
12. K. O. Koh and M. S. Jhon, Zeolites **5** (1985) 313.
13. K. O. Koh, H. Chon, and M. S. Jhon, J. Catal. **98** (1986) 126.
14. K. Fiedler, U. Lohse, J. Sauer, H. Stach, H. Thamm, and W. Schirmer, 5th International Conference on Zeolites.
15. M. Pruski, H. Ernst, H. Pfeifer, and B. Staudte, Chem. Phys. Lett. **119**(5) (1985) 412.
16. J. Karger, M. Bulow, G. R. Millward, and J. M. Thomas, Zeolites **6** (1986) 146.
17. D. Freude, J. Haase, and J. Klinowski, Chem. Phys. Lett. **133**(6) (1987) 491.
18. D. Freude, J. Haase, H. Pfeifer, D. Prager, and G. Scheller, Chem. Phys. Lett. **114**(2) (1985) 143.
19. U. Pingel, J. P. Amoureux, T. Anupold, F. Bauer, H. Ernst, C. Fernandez, D. Freude, and A. Samoson, Chem. Phys. Lett. **194** (1998) 345.
20. A. Gutsze, J. Kornatowski, H. Neels, W. Schmitz, and G. Finger, Crystal Res. Technol. **20**(2) (1985) 151.
21. J. Klinowski, Prog. Nucl. Mag. Res., Sp. **16** (1984) 237.
22. J. Klinowski, J. M. Thomas, C. A. Fyfe, and G. C. Gobbi, Nature **256** (1982) 533.
23. D. Müller, W. Gessner, H.-J. Behrens, and G. Scheler, Chem. Phys. Lett. **79** (1981) 59.
24. J. J. Pluth and J. V. Smith, J. Am. Chem. Soc. **104** (1982) 6977.
25. J. J. Pluth and J. V. Smith, J. Am. Chem. Soc. **105** (1983) 1192.
26. G. Engelhardt and D. Michel, *High-Resolution Solid-State NMR of Silicates and Zeolites*, Wiley, Chichester (1987).
27. C. A. Fyfe, G. C. Gobbi, J. S. Hartman, J. Klinowski, and J. M. Thomas, J. Phys. Chem. **86** (1982) 1247.
28. P. A. Howell, Acta Cryst. **13** (1960) 737.
29. A. Samoson, E. Kundla, and E. Lippmaa, J. Magn. Res. **49** (1982) 350.
30. D. Freude and H.-J. Behrens, Cryst. Res. Technol. **16** (1981) 3.
31. H. Oka, Y. Tokunaga, T. Okada, H. Ohki, and T. Okuda, Micr. Mesopor. Mat. **33** (1999) 257.
32. E. Lippmaa, A. Samoson, and M. Magi, J. Am. Chem. Soc. **108** (1986) 1730.